Journal of The Electrochemical Society, **159** (3) A238-A243 (2012)
0013-4651/2012/159(3)/A238/6/$28.00 © The Electrochemical Society

Concurrent Reaction and Plasticity during Initial Lithiation of Crystalline Silicon in Lithium-Ion Batteries

Kejie Zhao,[a,*] Matt Pharr,[a] Qiang Wan,[a,b,] Wei L. Wang,[a,c] Efthimios Kaxiras,[a,c] Joost J. Vlassak,[a] and Zhigang Suo[a,z]**

[a]*School of Engineering and Applied Sciences and* [c]*Department of Physics, Harvard University, Cambridge, Massachusetts 02138, USA*
[b]*Institute of Structural Mechanics, China Academy of Engineering Physics, Mianyang 621900, China*

In an electrochemical cell, crystalline silicon and lithium react at room temperature, forming an amorphous phase of lithiated silicon. The reaction front—the phase boundary between the crystalline silicon and the lithiated silicon—is atomically sharp. Evidence has accumulated recently that the velocity of the reaction front is limited by the rate of the reaction at the front, rather than by the diffusion of lithium through the amorphous phase. This paper presents a model of concurrent reaction and plasticity. We identify the driving force for the movement of the reaction front, and accommodate the reaction-induced volumetric expansion by plastic deformation of the lithiated silicon. The model is illustrated by an analytical solution of the co-evolving reaction and plasticity in a spherical particle. We derive the conditions under which the lithiation-induced stress stalls the reaction. We show that fracture is averted if the particle is small and the yield strength of lithiated silicon is low. Furthermore, we show that the model accounts for recently observed lithiated silicon of anisotropic morphologies.
 [DOI: 10.1149/2.020203jes]

Manuscript submitted July 22, 2011; revised manuscript received October 4, 2011. Published December 30, 2011.

Lithium-ion batteries dominate the market of power sources for wireless electronics, and are being implemented in electric vehicles.[1,2] Intense efforts are dedicated to developing next-generation lithium-ion batteries with high energy density, long cycle life, and safe operation.[3,4] Silicon can host a large amount of lithium, making it one of the most promising materials for anodes.[5] Lithiation of silicon, however, causes large volumetric expansion and mechanical stress, often leading to the shedding of active materials and rapid decay of capacity.[6] This mode of failure can be mitigated in nanostructured silicon anodes. Examples include nanowires,[7] thin films,[8] nanoporous structures,[9] hollow nano-particles,[10] and carbon-silicon composites.[11] Specifically, recent experiments and theories show that nanostructured silicon may avert fracture when the lithiation-induced expansion is accommodated by plasticity.[12–18] To develop such nanostructured anodes, it is urgent to understand lithiation-induced stress, deformation, and fracture.

Nanostructured electrodes of silicon are often fabricated with crystalline silicon. In an electrochemical cell, crystalline silicon and lithium react at room temperature, forming an amorphous phase of lithiated silicon [Fig. 1].[7,19–23] The reaction front is atomically sharp—the phase boundary between the crystalline silicon and the lithiated silicon has a thickness of ∼1 nm.[24] Evidence has accumulated recently that, in the nanostructured electrodes, the velocity of the reaction front is not limited by the diffusion of lithium through the amorphous phase, but by the reaction of lithium and silicon at the front. For example, it has been observed that under a constant voltage the displacement of the reaction front is linear in time.[25] This observation indicates that the rate of lithiation is limited by short-range processes at the reaction front, such as breaking and forming atomic bonds.

That the reaction is the rate-limiting step is perhaps most dramatically demonstrated by lithiated silicon of anisotropic morphologies. Recent experiments have shown that lithiated silicon grows preferentially in a direction perpendicular to the (110) planes of crystalline silicon.[25–27] It has been suggested that the anisotropic morphologies are due to the difference in diffusivities along various crystalline orientations of silicon. However, it is well established that the tensor of diffusivity of a species in a cubic crystal is isotropic.[28] We propose that the observed anisotropic morphologies are due to the variation in the short-range atomic processes at the reaction fronts in different crystallographic orientations.

We further note that, to accommodate the large volumetric expansion associated with the phase transition, the lithiated silicon must deform plastically. It is instructive to compare a flat reaction front with a curved one. When the reaction front is flat [Fig. 2a], the large volumetric expansion associated with the reaction is accommodated by elongating the lithiated silicon in the direction normal to the reaction front, while maintaining the geometric compatibility between the two phases in the directions tangential to the reaction front. As the reaction front advances, freshly lithiated silicon is added at the front, and previously lithiated silicon recedes by rigid-body translation, with no deformation. The biaxial stresses in the lithiated silicon remain at the compressive yield strength. When the reaction front is flat, reaction and plasticity are concurrent and co-locate—right at the reaction front. Indeed, the two processes may not be differentiated without ambiguity.

When the reaction front is curved, the crystalline silicon and the lithiated silicon form a core-shell structure [Fig. 2b]. As the reaction front advances, freshly lithiated silicon is added at the front, previously lithiated silicon recedes, and the shell enlarges. An element of lithiated silicon at the curved front initially undergoes compressive plastic deformation in the hoop directions. Upon subsequent lithiation of the core, the element is pushed away from the front, unloads elastically, and then deforms plastically in *tension* in the hoop directions. This process results in tensile hoop stress at the surface of the particle, possibly causing fracture. When the reaction front is curved, reaction and plasticity are concurrent, but can occur at different places. There is no ambiguity in differentiating processes at the reaction front and plastic deformation inside the lithiated silicon.

We present a model of concurrent reaction and plasticity. Existing analyzes of lithiation-induced deformation and fracture have assumed diffusion-limited lithiation.[15–17,29–36] Liu et. al. described a two-phase model with diffusivities dependence on local lithium concentration, giving an evolving core-shell structure with a sharp interface separating Li-deficient core and Li-rich shell.[31] In this paper, motivated by experimental observations, we assume that the velocity of the reaction front is limited by the rate of the reaction of lithium and silicon at the front, rather than by the diffusion of lithium through the amorphous phase. We identify the driving force for the movement of the phase boundary, and accommodate the reaction-induced volumetric expansion by plastic deformation of lithiated silicon. The model is illustrated by an analytical solution of the co-evolving reaction and plasticity in a spherical particle. We show that lithiation may induce high enough stress to stall the reaction, and that fracture is averted if the particle is small and the yield strength of lithiated silicon is low.

* Electrochemical Society Student Member.
** Electrochemical Society Active Member.
z E-mail: suo@seas.harvard.edu

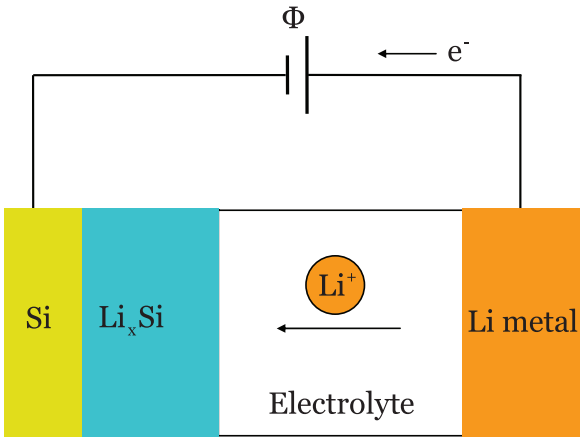

Figure 1. Schematic of an electrochemical test cell composed of a lithium metal anode and a crystalline silicon cathode. Crystalline silicon and lithium react at room temperature, forming an amorphous phase of lithiated silicon. The reaction front—the boundary between the crystalline silicon and the lithiated silicon—is atomically sharp.

Furthermore, we show that the model accounts for recently observed lithiated silicon of anisotropic morphologies.

A Model of Concurrent Reaction and Plasticity

Fig. 1 illustrates an electrochemical cell, in which crystalline silicon and lithium react and form an amorphous phase of lithiated silicon:

$$\mathrm{Li} + \frac{1}{x}\mathrm{Si} = \frac{1}{x}\mathrm{Li}_x\mathrm{Si}. \qquad [1]$$

The two electrodes are connected through a conducting wire and an electrolyte. The conducting wire may be connected to an external voltage source. At the interface between the lithium electrode and the electrolyte, lithium atoms dissociate into lithium ions and electrons. Lithium ions pass through the electrolyte, and electrons pass through the conducting wire. Since lithiated silicon is an electron conductor,[22] lithium ions and electrons recombine into lithium atoms upon reaching the silicon electrode. Lithium atoms then diffuse through the lithiated silicon, and react with the crystalline silicon—at the reaction front—to form fresh lithiated silicon. The reaction causes the lithiated silicon to grow at the expense of the crystalline silicon and metallic lithium.

Migration of lithium ions in the electrolyte is relatively fast, so that the diffusion of lithium through the lithiated silicon and the reaction between lithium and silicon at the front may limit the velocity of the reaction front. Let D be the diffusivity of lithium in the lithiated silicon, V the velocity of the reaction front, and L the thickness of the lithiated silicon. These quantities form a dimensionless group:

$$\chi = \frac{D}{VL}. \qquad [2]$$

The parameter χ characterizes the relative rate of diffusion and reaction. If χ is large, the diffusion of lithium is fast, and lithiation is limited by the reaction. A representative value of diffusivity of lithium at room temperature in lithiated silicon is $D = 10^{-16}\mathrm{m}^2/\mathrm{s}$.[37,38] A reported velocity of the reaction front of the lithiation of a (100)-Si wafer is $V = 1.2 \times 10^{-11}\mathrm{m/s}$.[24] We note that the reaction velocity may be dependent on the crystallographic directions.[25,26] So far, a systematic experimental study of such dependence is incomplete. For rates of diffusion and reaction to be comparable, $\chi = 1$, and the thickness of the lithiated silicon is calculated to be $L = 8\,\mu m$. In typical nanostructured electrodes of silicon, the feature size is less than a few hundreds of nanometers.[7–11] Thus, for electrodes at such size scales, the velocity of the reaction front is limited by the reaction of silicon and lithium at the front, rather than by the diffusion of lithium through the amorphous phase.

We next identify the driving force for the reaction, namely, the change in the free energy associated with the reaction that converts one lithium atom and $1/x$ number of silicon atoms into lithiated silicon. Let ΔG_r be the free energy of reaction 1 when both the stress and the applied voltage vanish. When the conducting wire is connected through a voltage source, associated with converting one lithium atom into lithiated silicon, one electron passes through the conducting wire, so that the external voltage source does work $e\Phi$, where Φ is the voltage, and $e$is the elementary charge (a positive quantity). The driving force is further modified when the two phases, the crystalline silicon and the lithiated silicon, are stressed. (The metallic lithium electrode is taken to be stress-free.) Associated with converting one lithium atom into lithiated silicon, the crystalline silicon phase loses $1/x$ number of silicon atoms, and the stress in silicon does work $-\sigma_m^{\mathrm{Si}}\Omega^{\mathrm{Si}}/x$, where σ_m^{Si} is the mean stress in silicon at the reaction front, and Ω^{Si} is the volume per silicon atom. The amorphous phase gains $1/x$ number of silicon atoms and one lithium atom, so that the stress in the amorphous phase does work $\sigma_m^{\mathrm{Li_xSi}}\Omega^{\mathrm{Li_xSi}}/x$, where $\sigma_m^{\mathrm{Li_xSi}}$ is the mean stress in the amorphous phase at the reaction front, and $\Omega^{\mathrm{Li_xSi}}$ is the volume per unit of $\mathrm{Li_xSi}$.

Combining the above contributions, we find that, when the reaction advances by converting one lithium atom and $1/x$ number of silicon atoms into lithiated silicon, the net change in the free energy is

$$\Delta G = \Delta G_r - e\Phi + \frac{1}{x}\left(\sigma_m^{\mathrm{Si}}\Omega^{\mathrm{Si}} - \sigma_m^{\mathrm{Li_xSi}}\Omega^{\mathrm{Li_xSi}}\right). \qquad [3]$$

We have neglected the dissipation at electrolyte/electrode interfaces, as well as inside the electrodes and electrolytes. In our sign convention, a negativeΔG drives lithiation, and a more negative value represents a larger driving force. The free energy of reaction ΔG_r takes a negative value. In Fig. 1, we have drawn the polarity of the voltage source in the direction that drives lithiation. As expected, a compressive mean stress in the crystalline silicon promotes lithiation, but a compressive mean stress in the lithiated silicon retards lithiation.

This net change in the free energy is the driving force for the movement of the reaction front. The velocity of the reaction front will increase as the magnitude of the driving force increases. The reaction is taken to be thermally-activated, described by the familiar kinetic model:[39]

$$V = V_0 \exp\left(-\frac{Q}{kT}\right)\left[\exp\left(-\frac{\Delta G}{kT}\right) - 1\right], \qquad [4]$$

where kT is the temperature in the unit of energy, Q the activation energy, and V_0 a parameter analogous to the exchange current density in a redox process. The velocity of the reaction is taken to be positive when the crystalline silicon is consumed and the lithiated silicon grows. When $\Delta G = 0$, the electrochemical cell is in equilibrium, and the reaction halts, $V = 0$. When $\Delta G < 0$, the reaction front advances in the direction that consumes crystalline silicon, $V > 0$. When ΔG

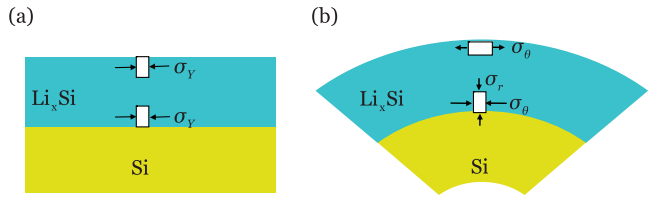

Figure 2. The lithiation of silicon causes a large volumetric expansion, which is accommodated by plastic deformation. (a) In a thin film with no curvature, as the reaction front advances, freshly lithiated silicon is added at the front, and previously lithiated silicon recedes by rigid-body translation, with no deformation. The biaxial stresses in the lithiated silicon remain at the compressive yield strength. (b) At a curved reaction front, an element of newly lithiated silicon undergoes compressive plastic deformation in the directions tangent to the reaction front. As the reaction front advances, the element is pushed away from the front, unloads elastically, and then undergoes tensile plastic deformation in the directions tangential to the reaction front. The external surface of the lithiated silicon is subject to tensile hoop stress, possibly leading to fracture.

> 0, it may seem that the reverse reaction would take place—the lithiated phase would be consumed, Si redeposited at the reaction front, and Li redeposited as lithium metal. The reaction front would move in the direction opposite as that during lithiation. However, experiments have suggested that during delithiation ($\Delta G > 0$), the phase boundary remains stationary as Li is removed from the amorphous layer.[24] Thus, the forward and backward reactions seem to involve distinct kinetic processes. Such complication should be considered in describing an accurate kinetic model. Nevertheless, in the case of $|\Delta G| >> kT$, as is common in these systems at room temperature, the forward reaction is more prominent than the backward one. Thus, the kinetics model of Eq. 4, based on transition state theory, is still approximately valid.

At this writing, the available experimental data are lacking in completeness to substantiate kinetic model of any specific form. As such, in the following sections, we calculate the stress field and simulate the morphology of lithiated silicon with a prescribed velocity field. The considerations in Eq. 3–4 may aid the planning of future experiments.

Associated with the reaction 1, the volume of the silicon electrode expands by the ratio

$$\beta = \frac{\Omega^{\mathrm{Li_xSi}}}{\Omega^{\mathrm{Si}}}. \qquad [5]$$

The lithiation-induced expansion is too large to be accommodated by elastic deformation; rather, the large lithiated-induced expansion is accommodated by plastic deformation of the lithiated silicon.[12–18] The concurrent reaction and plasticity evolve a field of stress in both crystalline and lithiated silicon. The reaction front is atomically sharp, the amorphous phase attains the fully lithiated state, and the crystalline silicon core remains free of lithium.[24] The crystalline silicon is modeled as an elastic material, and the lithiated silicon is modeled as an elastic-plastic material.[13,15–17] The elastic-plastic model can be found in the classic text of Hill.[40]

The models of reaction kinetics and elastic-plastic deformation, in combination, co-evolve the reaction front and elastic-plastic field. At a given time, the location of the reaction front and the elastic-plastic field are known. For a small increment in time, advance the reaction front by an amount following the kinetic model, and then accommodate the reaction-induced volumetric expansion by updating the elastic-plastic field. Repeat the procedure to trace the co-evolution incrementally in time.

Lithiation of a Spherical Particle of Crystalline Silicon

To illustrate the salient features of the model, we derive an analytical solution of a spherical particle. A particle of pristine crystalline silicon, radius B, is taken to be the reference configuration [Fig. 3a]. The velocity of the reaction front is taken to be the same everywhere on the front, so that the front remains to be a spherical surface as it advances, and the spherical symmetry is retained. The magnitude of the velocity, however, may change as the reaction progresses. At time t, Fig. 3b, the particle becomes a core-shell structure, with the radius of the crystalline core being A, and the outer radius of the amorphous shell being $b(t)$. The function $A(t)$ specifies the extent of reaction, and the velocity of the reaction front is $V = -dA(t)/dt$. In the reference configuration, an element of crystalline silicon is identified by the radius R. At time t, this element is lithiated and moves to a place of radius r. The function $r(R, t)$ specifies the field of deformation. In representing a field, we may choose either R or r as an independent variable. One variable can be changed to the other by using the function $r(R, t)$. We will indicate our choice in each field explicitly when the distinction is important.

Elastic strain is much smaller than the volumetric strain associated with the phase transition. To focus on the main ideas, we neglect elastic strains of both phases, and model the crystalline silicon as a rigid material, and the lithiated silicon as a rigid-plastic material.[40] Consequently, the expansion of the particle is entirely due to lithiation. Consider the shell of the lithiated silicon between the radii A and r. This shell is lithiated from the shell of the pristine crystalline silicon

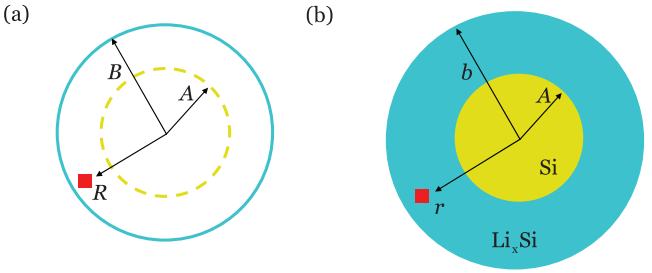

Figure 3. Lithiation of a spherical particle of crystalline silicon. (a). The pristine crystalline silicon, radius B, is taken as the reference configuration, in which a spherical surface is marked by the radius A, and an element of silicon by the radius R. (b). At time t, silicon in the shell outside the radius A is lithiated, and the element R moves to a new position of radius r.

between the radii A and R. The ratio of the volume of the lithiated shell over the volume of the crystalline shell is β, so that

$$r^3 - A^3 = \beta(R^3 - A^3). \qquad [6]$$

This equation gives the function $r(R, t)$ once the function $A(t)$ is given. That is, $A(t)$ fully specifies the kinematics of the spherical particle. In particular, the outer radius of the lithiated silicon is obtained by setting $R = B$ in 6:

$$b = [A^3 + \beta(B^3 - A^3)]^{1/3}. \qquad [7]$$

The radial and hoop stretches can be calculated from

$$\lambda_r = \frac{\partial r(R, t)}{\partial R}, \quad \lambda_\theta = \frac{r(R, t)}{R}. \qquad [8]$$

The crystalline core is in a state of homogeneous hydrostatic compression. The stress field in the amorphous shell, however, is inhomogeneous. Each material element in the shell is subject to a state of triaxial stresses. Let σ_r be the radial stress, and σ_θ the hoop stress [Fig. 4a]. We adopt a commonly used idealization that plastic deformation is unaffected when a hydrostatic stress is superposed. Superposing a hydrostatic stress of magnitude σ_r, we observe that the state of plastic deformation of the element subject to the triaxial stresses is

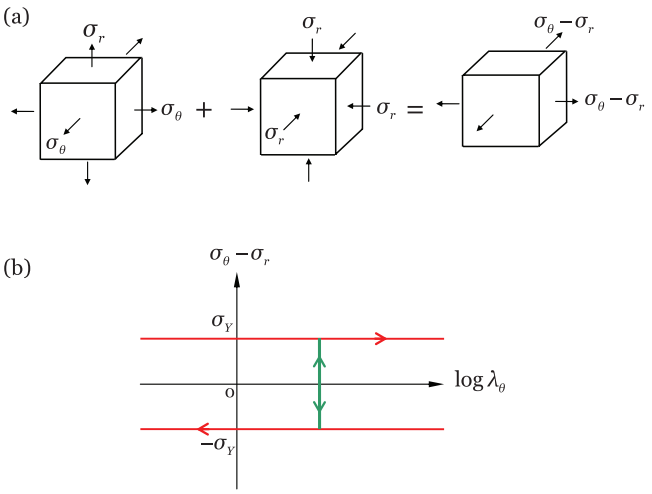

Figure 4. (a) The state of plastic deformation of an element subject to the triaxial stresses $(\sigma_r, \sigma_\theta, \sigma_\theta)$ is the same as that of an element subject to equal-biaxial stresses $\sigma_\theta - \sigma_r$. (b) The stress-strain relation in terms of the stress $\sigma_\theta - \sigma_r$ and the strainlog λ_θ. When $\sigma_\theta - \sigma_r = +\sigma_Y$, the plastic deformation is tensile in the hoop direction. When $\sigma_\theta - \sigma_r = -\sigma_Y$, the plastic deformation is compressive in the hoop direction. The elastic strain is negligible compared to lithiated strain, so that elastic part of the stress-strain relation is represented by a vertical line.

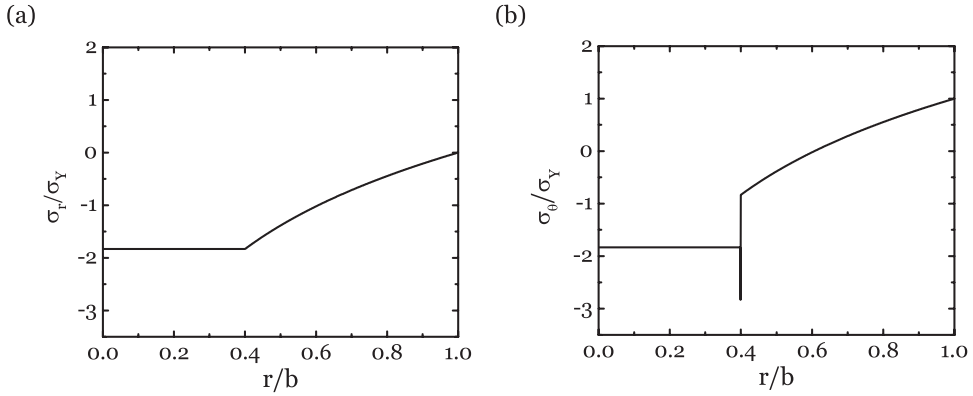

Figure 5. Stress field in a spherical particle when the reaction front is at $A/b = 0.4$. (a) radial stress, (b) hoop stress.

the same as the state of the plastic deformation of the element subject to equal biaxial stresses, $\sigma_\theta - \sigma_r$.

Fig. 4b sketches the stress-stretch relation in terms of the stress $\sigma_\theta - \sigma_r$ and the strain $\log \lambda_\theta$. For simplicity, the yield strength of the lithiated phase, σ_Y, is taken to be constant, independent of the amount of deformation and the concentration of lithium. An element of newly lithiated silicon is compressed in the hoop directions, and is in the state $\sigma_\theta - \sigma_r = -\sigma_Y$. Subsequently, this material element is pushed outward by even newer lithiated silicon, and undergoes elastic unloading. Because the elastic strain is negligible compared to lithiation-induced strain, the elastic unloading is represented by the vertical line in Fig. 4b. After elastic unloading, and element plastically deforms under $\sigma_\theta - \sigma_r = +\sigma_Y$.

The balance of forces acting on a material element requires that

$$\frac{\partial \sigma_r(r,t)}{\partial r} + 2\frac{\sigma_r(r,t) - \sigma_\theta(r,t)}{r} = 0. \qquad [9]$$

Setting $\sigma_\theta - \sigma_r = \sigma_Y$ in 9 and integrating over r with the traction-free boundary condition, $\sigma_r(b,t) = 0$, we obtain the radial stress in the shell:

$$\sigma_r = -2\sigma_Y \log(b/r), \quad A \le r \le b. \qquad [10]$$

The hoop stress inside the shell, away from the reaction front, is determined from $\sigma_\theta - \sigma_r = \sigma_Y$, giving

$$\sigma_\theta = \sigma_Y - 2\sigma_Y \log(b/r), \quad A < r \le b. \qquad [11]$$

As discussed above in connection with Fig. 2, in the shell at the reaction front, the element of the freshly lithiated silicon undergoes plastic deformation, which elongates the element in the radial direction. The hoop stress in the element of freshly lithiated silicon is determined from $\sigma_\theta - \sigma_r = -\sigma_Y$, giving

$$\sigma_\theta = -\sigma_Y - 2\sigma_Y \log(b/A), \quad r = A. \qquad [12]$$

A comparison of 11 and 12 indicates a jump in the hoop stress by magnitude $2\sigma_Y$. This jump is caused by our neglecting the elastic strain. Should we include elastic strain, the hoop stress would make a transition from 12 to 11 within a very thin shell.

As mentioned above, the core is in a state of homogeneous and hydrostatic compression. In order to balance forces, the radial stress is continuous across the reaction front. Setting $r = A$ in 10, we obtain the stress field in the crystalline core:

$$\sigma_r = \sigma_\theta = -2\sigma_Y \log(b/A), \quad r \le A. \qquad [13]$$

Fig. 5 plots the stress field when the reaction front is at $A/b = 0.4$. As expected, the core is in a homogeneous state of hydrostatic compression, but the stress field in the shell is triaxial and inhomogeneous. The radial stress in the shell is compressive, with $\sigma_r(b,t) = 0$ prescribed as the boundary condition. Because of the triaxial state of stress, the magnitude of the stress component readily exceeds the yield strength. The hoop stress is tensile at the external surface of the particle, $\sigma_\theta(b,t) = \sigma_Y$, and gradually becomes compressive inside the shell. Near the reaction front, the hoop stress jumps by amplitude $2\sigma_Y$, as discussed before.

For the spherical particle, the field of stress and the field of deformation are fully determined once the radius of the core A is specified. We now examine how the stress affects the movement of the reaction front. The mean stress in the crystalline silicon is $\sigma_m^{Si} = -2\sigma_Y \log(b/A)$. At the reaction front, the mean stress in the lithiated silicon is $\sigma_m^{Li_xSi} = -2\sigma_Y \log(b/A) - 2\sigma_Y/3$. Inserting these expressions into 3, we obtain the driving force for the movement of the reaction front:

$$\Delta G = \Delta G_r - e\Phi + \frac{2\sigma_Y \Omega^{Si}}{x}\left[(\beta - 1)\log\left(\frac{b}{A}\right) + \frac{\beta}{3}\right]. \qquad [14]$$

The contribution due to the stresses is plotted in Fig. 6, where the horizontal axis is the normalized radius of the crystalline core A/b. In making this plot, we have adopted the following values: $\beta = 4$,[6] $x = 3.75$,[24] $\sigma_Y = 1$GPa,[13] and $\Omega^{Si} = 2.0 \times 10^{-29}$m^3.[23] As expected, the contribution due to the stresses is positive and retards lithiation. The magnitude of the contribution increases as the crystalline core shrinks. Recall that the free energy of formation of lithiated silicon is small; for example, $\Delta G_r = -0.18$ eV for amorphous $Li_{2.1}Si$.[19] Consequently, the reaction can readily generate large enough stress to counteract the electrochemical driving force, stalling the reaction. Note that the free energy of reaction ΔG_r differs for amorphous Li-Si phases with various Li compositions; the experimental data on such functional dependence is unavailable to date.

The curvature of the electrode plays a key role in this contribution of the stress to the free energy. To illustrate this point, consider a

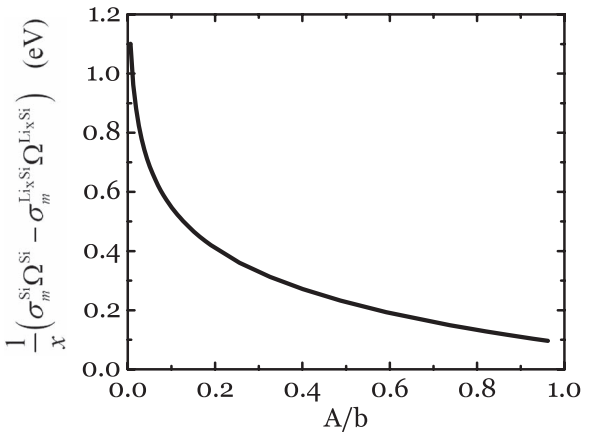

Figure 6. The contribution of the stress to the driving force of lithiation is plotted as a function of the normalized radius of the core.

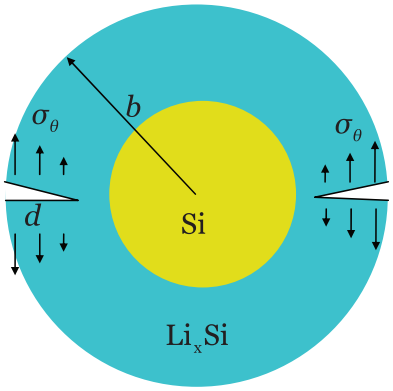

Figure 7. A preexisting circumferential crack in a spherical particle of electrode.

flat crystalline silicon electrode. In the initial stages of lithiation, the amorphous phase exists as a thin film on a crystalline silicon substrate. As previously mentioned, the biaxial stress in the freshly lithiated silicon is at the compressive yield strength. The stress in the crystalline silicon is zero. Using the same representative values as for the spherical particle, the contribution from the stress to the free energy in 3 is 0.089 eV. As with the spherical particle, in a thin film, the stresses retard lithiation. However, the value of this contribution is small compared to the values found for the spherical particle [Fig. 6]. Hence, the curvature can greatly influence the rate of lithiation of crystalline silicon.

Reaction-Induced Fracture

We now analyze reaction-induced fracture using an approach similar to that described in several recent papers.[41–43] We focus on fracture caused by the tensile hoop stress during the lithiation of a spherical particle of silicon. A circumferential crack, depth d, is assumed to preexist in the particle, as illustrated in Fig. 7. We ask if the lithiation-induced stress will cause the crack to grow. The propagation of the crack, should it occur, is assumed to be a much faster process than the plastic flow. Consequently, in analyzing fracture, we assume that no further plastic deformation occurs during the propagation of the crack, and we adopt linear elastic fracture mechanics. The reduction in the elastic energy associated with the crack advancing a unit area defines the energy release rate G. Dimensional analysis dictates that the energy release rate should take the form[44]

$$G = Z\frac{\sigma_Y^2}{E}b, \qquad [15]$$

where E is Young's modulus, and Z is a dimensionless number to be determined by solving the elastic boundary-value problem. At a given time, once the location and the depth of the crack are given, Z is uniquely determined. For the lithiation of a spherical particle, the energy release reaches the maximum value when the particle is fully lithiated, and the length of the crack equals the size of the regime where hoop stress is tensile, $d/b = 0.395$. Therefore, the calculation gives a conservative critical particle size to avoid fracture. We use the commercial finite-element software ABAQUS to calculate the energy release rate. In the simulation, we input the stress distribution at the fully lithiated state, and the J-integral is used to calculate the energy release rate. Our calculation gives $Z = 0.91$.

Let Γ be the fracture energy of the particle. No preexisting flaws will advance if the maximum energy release rate is below the fracture energy. Thus, 15 defines a critical particle size:

$$b_{cr} = \frac{\Gamma E}{Z\sigma_Y^2}. \qquad [16]$$

When the size of the particle is below this critical value, fracture is averted. That is, fracture is averted if the particle is small and the yield strength is low. Taking representative values, $\Gamma = 10\,\mathrm{J/m^2}$,[15] $E = 35\,\mathrm{GPa}$,[45] and $\sigma_Y = 1\,\mathrm{GPa}$,[13] we find that the critical radius of fully lithiation silicon is $b_{cr} = 380\,\mathrm{nm}$. The critical radius of the pristine crystalline silicon is thus $B_{cr} = 239\,\mathrm{nm}$. The size dependent fracture of crystalline silicon nanoparticles during lithiation has also been evident in in-situ TEM experiments.[31]

Lithiated Silicon Of Anisotropic Morphologies

Recent experiments have shown that electrochemical reaction of crystalline silicon and lithium produces lithiated silicon of fascinating morphologies.[25–27] Lee et al. have fabricated nanopillars of crystalline silicon, of axial orientations ⟨100⟩, ⟨110⟩ and ⟨111⟩, all with circular cross sections. On lithiation, the cross sections of these nanopilars evolve into crosses, ellipses and hexagons, respectively.[27] Liu et al. have reported that a nanowire of crystalline silicon, of ⟨112⟩ axial orientation, upon lithiation, evolves into a wire of a dumbbell-shaped cross section.[25] Goldman et al. have fabricated arrays of micron-sized structures of crystalline silicon—bars, posts and platelets—and shown that lithiated silicon grows predominantly along the ⟨110⟩ orientations of silicon, and negligibly along the ⟨111⟩ orientations.[26]

It has been suggested that the anisotropic morphologies are due to the difference in diffusivities along various crystalline orientations of silicon. This suggestion contradicts a mathematical theorem: the tensor of diffusivity of a species in a cubic crystal is isotropic.[28] Instead, we propose that the observed anisotropic morphologies are due to different rates of reaction on various surfaces of crystalline silicon. Lithiation of crystalline silicon is a heterogeneous reaction: lithium and silicon react on the surfaces of crystalline silicon. For this heterogeneous reaction to advance, corporative rearrangement of atoms must occur. Surfaces of silicon in various crystallographic orientations have drastically different atomic structures. It seems plausible that such pronounced dissimilarity in the atomic structures on various surfaces of crystalline surface can readily result in different rates of reaction on these surfaces.

For heterogeneous reactions involving single crystals, anisotropy in the rates of reaction is a norm, rather than an exception. Lithiation of crystalline silicon, however, is of particular interest because this reaction generates an exceptionally large volumetric expansion, and because intriguing experimental observations are being reported. In the absence of a detailed atomistic model of the anisotropy of the lithiation reaction, we proceed as follows, within the model of concurrent reaction and plasticity. We take the experimentally observed anisotropic morphologies as a basis to ascribe different velocities to reaction fronts in different crystallographic orientations. The freshly lithiated silicon at these reaction fronts push previously lithiated silicon, which then undergoes plastic deformation to accommodate the volumetric expansion associated with the freshly lithiated silicon. The concurrent reaction and plasticity evolve the anisotropic morphologies.

To illustrate this model, we simulate the morphological evolution observed during the lithiation of a crystalline silicon nanopillar.[27] Fig. 8a shows the cross section of a silicon nanopillar with different crystallographic facets. The diameter of the nanopillar is around 100 nm.[27] The concurrent reaction and plasticity are simulated by using ABAQUS. The lithiation-induced volumetric expansion is simulated as if it were thermal expansion, while deformation in the lithiated silicon is modeled by the elastic-plastic theory.[40] To simulate the movements of the reaction fronts, we prescribe a moving temperature field. The velocity of the front depends on the crystallographic orientation. Following the experimental observation, we assume that reaction primarily occurs on the (110) crystalline facets.[26] The simulation advances incrementally in time. At a given time, all reaction fronts are at the known positions. The volumetric expansion associated with the freshly lithiated silicon is simulated within ABAQUS by prescribing a change in temperature. To accommodate this volumetric expansion, the plastic deformation is updated by solving the

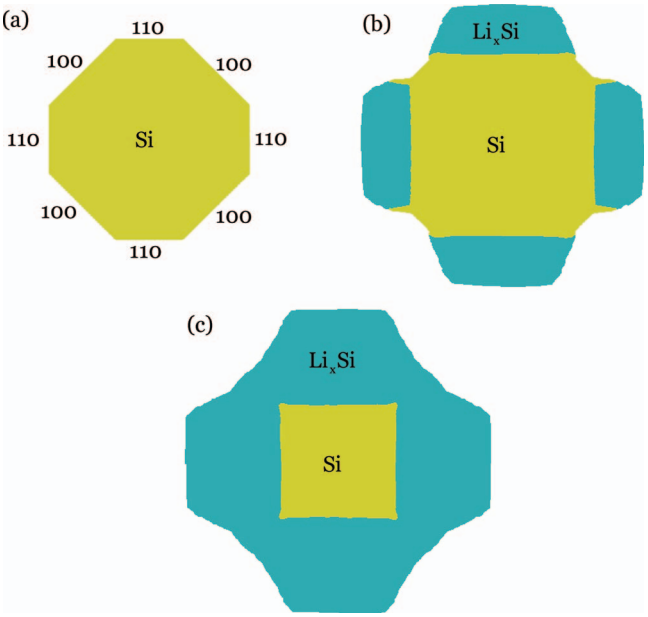

Figure 8. Concurrent migration of the reaction front and plastic deformation in the amorphous phase evolve the anisotropic shape. (a) Schematics of silicon electrode with different crystallographic facets. Lithiation reaction primarily occurs on the ⟨110⟩ planes. The anisotropic shape evolution at the time (b) $t/\tau = 0.25$, and (c) $t/\tau = 0.5$. τ is the time to fully lithiate the crystalline silicon particle.

boundary-value problem. To avoid computational singularity, the temperature front, which simulates the reaction front, is located within a thin shell, whose size is much smaller than the feature size of the nanopillar, but sufficiently larger than the mesh size. Such regularization is used to afford a compromise between computational cost and accuracy. Fig. 8b and 8c show the morphologies of the particle at two stages of reaction, $t/\tau = 0.25$ and $t/\tau = 0.5$, using the procedure described above. τ is the time to fully lithiate the crystalline silicon particle. The anisotropic pattern agrees well with the experimental observation.[27]

Conclusions

Crystalline silicon and lithium react to form lithiated silicon. The reaction front is at the atomically sharp phase boundary between the crystalline silicon and lithiated silicon. The reaction generates a large volumetric expansion, which is accommodated by plastic deformation in the lithiated silicon. This paper describes a model that co-evolves the reaction front and plastic deformation. The velocity of the reaction front relates to the change in the free energy through a kinetic model, while the stress field evolves according to the elastic-plastic theory. The model is illustrated with the lithiation of a spherical particle of crystalline silicon. We show that fracture is averted when the particle is small and the yield strength of lithiated silicon is low. The model also accounts for anisotropic morphologies of lithiated silicon. It is hoped that model will aid in the planning of future experiments and atomistic simulations.

Acknowledgments

This work is supported by the National Science Foundation through a grant on Lithium-ion Batteries (CMMI-1031161). MP acknowledges government support under and awarded by DoD, Air Force Office of Scientific Research, National Defense Science and Engineering Graduate (NDSEG) Fellowship, 32 CFR 168a.

References

1. M. Armand and J. M. Tarascon, *Nature*, **451**, 652 (2008).
2. R. F. Service, *Science*, **332**, 1494 (2011).
3. B. L. Ellis, K. T. Lee, and L. F. Nazar, *Chem. Mat.*, **22**, 691 (2010).
4. R. Marom, S. F. Amalraj, N. Leifer, D. Jacob, and D. Aurbach, *J. Mater. Chem.*, **21**, 9938 (2011).
5. W. J. Zhang, *J. Power Sources*, **196**, 13 (2011).
6. L. Y. Beaulieu, K. W. Eberman, R. L. Turner, L. J. Krause, and J. R. Dahn, *Electrochem. Solid ST.*, **4**, A137 (2001).
7. C. K. Chan, H. L. Peng, G. Liu, K. McIlwrath, X. F. Zhang, R. A. Huggins, and Y. Cui, *Nat. Nanotechnol.*, **3**, 31 (2008).
8. T. Takamura, S. Ohara, M. Uehara, J. Suzuki, and K. Sekine, *J. Power Sources*, **129**, 96 (2004).
9. L. Baggetto, D. Danilov, and P. H. L. Notten, *Adv. Mater.*, **23**, 1563 (2011).
10. Y. Yao, M. T. McDowell, I. Ryu, H. Wu, N. Liu, L. B. Hu, W. D. Nix, and Y. Cui, *Nano Lett.*, **11**, 2949 (2011).
11. M. Yamada, A. Ueda, K. Matsumoto, and T. Ohzuku, *J. Electrochem. Soc.*, **158**, A417 (2011).
12. B. Hertzberg, A. Alexeev, and G. Yushin, *J. Am. Chem. Soc.*, **132**, 8548 (2010).
13. V. A. Sethuraman, M. J. Chon, M. Shimshak, V. Srinivasan, and P. R. Guduru, *J. Power Sources*, **195**, 5062 (2010).
14. J. Y. Huang, L. Zhong, C. M. Wang, J. P. Sullivan, W. Xu, L. Q. Zhang, S. X. Mao, N. S. Hudak, X. H. Liu, A. Subramanian, H. Y. Fan, L. A. Qi, A. Kushima, and J. Li, *Science*, **330**, 1515 (2010).
15. K. J. Zhao, M. Pharr, J. J. Vlassak, and Z. G. Suo, *J. Appl. Phys.*, **109**, 016110 (2011).
16. K. J. Zhao, M. Pharr, S. Q. Cai, J. J. Vlassak, and Z. G. Suo, *J. Am. Ceram. Soc.*, **94**, S226 (2011).
17. A. F. Bower, P. R. Guduru, and V. A. Sethuraman, *J. Mech. Phys. Solids*, **59**, 804 (2011).
18. S. K. Soni, B. W. Sheldon, X. C. Xiao, and A. Tokranov, *Scr. Mater.*, **64**, 307 (2011).
19. P. Limthongkul, Y. I. Jang, N. J. Dudney, and Y. M. Chiang, *Acta Mater.*, **51**, 1103 (2003).
20. M. N. Obrovac, and L. Christensen, *Electrochem. Solid ST.*, **7**, A93 (2004).
21. H. Li, X. J. Huang, L. Q. Chen, G. W. Zhou, Z. Zhang, D. P. Yu, Y. J. Mo, and N. Pei, *Solid State Ion.*, **135**, 181 (2000).
22. W. H. Wan, Q. F. Zhang, Y. Cui, and E. G. Wang, *J. Phys.-Condens. Mat.*, **22**, 415501 (2010).
23. K. J. Zhao, W. L. Wang, J. Gregoire, M. Pharr, Z. G. Suo, J. J. Vlassak, and E. Kaxiras, *Nano Lett.*, **11**, 2962 (2011).
24. M. J. Chon, V. A. Sethuraman, A. McCormick, V. Srinivasan, and P. R. Guduru, *Phys. Rev. Lett.*, **107**, 045503, 2011.
25. X. Liu, H. Zheng, L. Zhong, S. Huang, K. Karki, L. Q. Zhang, Y. Liu, A. Kushima, W. T. Liang, J. W. Wang, J. H. Cho, E. Epstein, S. A. Dayeh, S. T. Picraux, T. Zhu, J. Li, J. P. Sullivan, J. Cumings, C. S. Wang, S. Mao, Z. Z. Ye, S. L. Zhang, and J. Y. Huang, *Nano Lett.*, **11**, 3312 (2011).
26. J. L. Goldman, B. R. Long, A. A. Gewirth, and R. G. Nuzzo, *Adv. Funct. Mater.*, **21**, 2412 (2011).
27. S. W. Lee, M. T. McDowell, J. W. Choi, and Y. Cui, *Nano Lett.*, **11**, 3034 (2011).
28. J. F. Nye, *Physical Properties of Crystals: Their Representation by Tensors and Matrices*, P. 22, (Oxford University Press, New York 1985).
29. Y. T. Cheng and M. W. Verbrugge, *J. Electrochem. Soc.*, **157**, A508 (2010).
30. H. Haftbaradaran, J. Song, W. A. Curtin, and H. J. Gao, *J. Power Sources*, **196**, 361 (2010).
31. X. H. Liu, L. Zhong, S. Huang, S. X. Mao, T. Zhu, and J. Y. Huang, "Size Dependent Fracture of Silicon Nanoparticles during Lithiation", submitted, 2011.
32. I. Ryu, J. W. Choi, Y. Cui, and W. D. Nix, *J. Mech. Phys. Solids*, **59**, 1717 (2011).
33. V. R. Subramanian and R. E. White, *J. Power Sources*, **96**, 385 (2001).
34. V. R. Subramanian, H. J. Ploehn, and R. E. White, *J. Electrochem. Soc.*, **147**, 2868 (2000).
35. S. Renganathan, G. Sikha, S. Santhanagopalan, and R. E. White, *J. Electrochem. Soc.*, **157**, A155 (2010).
36. R. Deshpande, Y.-T. Cheng, M. W. Verbrugge, and A. Timmons, *J. Electrochem. Soc.*, **158**, A718 (2011).
37. N. Ding, J. Xu, Y. X. Yao, G. Wegner, X. Fang, C. H. Chen, and I. Lieberwirth, *Solid State Ion.*, **180**, 222 (2009).
38. J. Xie, N. Imanishi, T. Zhang, A. Hirano, Y. Takeda, and O. Yamamoto, *Mater. Chem. Phys.*, **120**, 421 (2010).
39. J O'M Bockris, A. K.N. Reddy, M. Gamboa-Aldeco, *Modern Electrochemistry, Vol. 2A, Fundamentals of Electrodics*, 2nd ed., Kluwer Academic/Plenum Publishers (2000).
40. R. Hill, *The Mathematical Theory of Plasticity*, (Oxford University Press, Oxford 1950).
41. K. J. Zhao, M. Pharr, J. J. Vlassak, and Z. G. Suo, *J. Appl. Phys.*, **108**, 073517 (2010).
42. Y. H. Hu, X. H. Zhao, and Z. G. Suo, *J. Mater. Res.*, **25**, 1007 (2010).
43. W. H. Woodford, Y.-M. Chiang, and W. C. Carter, *J. Electrochem. Soc*, **157**, A1052 (2010).
44. J. W. Hutchinson and Z. Suo, *Adv. Appl. Mech.*, **29**, 63 (1991).
45. V. A. Sethuraman, M. J. Chon, M. Shimshak, N. Van Winkle, and P. R. Guduru, *Electrochem. Commun.*, **12**, 1614 (2010).